HHS Public Access

Author manuscript

Anal Chem. Author manuscript; available in PMC 2020 January 02.

Published in final edited form as:

Anal Chem. 2018 September 18; 90(18): 10943–10950. doi:10.1021/acs.analchem.8b02468.

In vivo Chemical Monitoring at High Spatiotemporal Resolution using Microfabricated Sampling Probes and Droplet-Based Microfluidics Coupled to Mass Spectrometry

Thitaphat Ngernsutivorakul[a], **Daniel J. Steyer**[a], **Alec C. Valenta**[a], **Robert T. Kennedy**[a,b,*]

[a]Department of Chemistry, University of Michigan, 930 N. University Ave, Ann Arbor, MI 48109

[b]Department of Pharmacology, University of Michigan, 1150 W. Medical Center Drive, Ann Arbor, MI 48109

Abstract

An essential approach for *in vivo* chemical monitoring is to use sampling probes coupled with analytical methods; however, this method traditionally has limited spatial and temporal resolution. To address this problem, we have developed an analytical system that combines microfabricated push-pull sampling probes with droplet-based microfluidics. The microfabricated probe provides approximately 1000-fold better spatial resolution than common microdialysis probes. Microfabrication also facilitated integration of an extra channel into the probe for microinjection. We have created microfluidic devices and interfaces that allowed manipulating nanoliter droplet samples collected from the microfabricated probe at intervals of a few seconds. Use of droplet-based microfluidics prevented broadening of collected zones, yielding 6 s temporal resolution at 100 nL/min perfusion rates. Resulting droplets were analyzed by direct infusion nanoelectrospray ionization (nESI) mass spectrometry for simultaneous determination of glutamine, glutamate, γ-aminobutyric acid, and acetylcholine. Use of low infusion rates that enabled nESI (50 nL/min) was critical to allowing detection in the complex samples. Addition of ^{13}C-labeled internal standards to the droplet samples was used for improved quantification. Utility of the overall system was demonstrated by monitoring dynamic chemical changes evoked by microinjection of high potassium concentrations into the brain of live rats. The results showed stimulated neurochemical release with rise times of 15 s. This work demonstrates the potential of coupling microfabricated sampling probes to droplet-based mass spectrometric assays for studying chemical dynamics in a complex microenvironment at high spatiotemporal resolution.

Graphical Abstract

*Corresponding author (rtkenn@umich.edu).

CONFLICT OF INTEREST

The authors declare no competing financial interest.

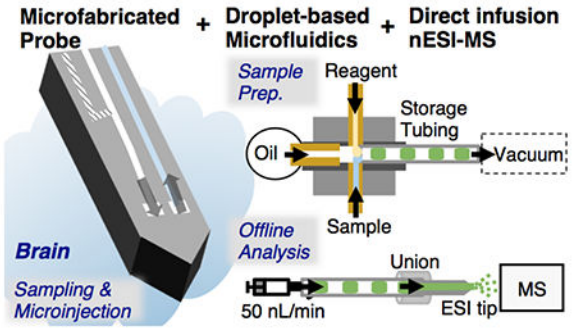

INTRODUCTION

Measuring the concentration dynamics of neurotransmitters and metabolites *in vivo* is a powerful way to investigate brain function[1–5]. Techniques such as microdialysis sampling[6–8], electrochemical sensors[9,10], genetically-encoded sensors[11,12], and positron emission tomography[13,14] have all been used for this purpose. An ideal method would allow high temporal and spatial resolution, be minimally invasive, allow multiple component measurements, and have easily tuned selectivity for sensing. None of the techniques currently in use fully meets this ideal; but, each has significant strengths so that the methods are largely complementary. Sensors have excellent temporal and spatial resolution but tuning the selectivity and measuring several compounds at once are significant challenges. Microdialysis allows multicomponent measurements and easily tuned selectivity; however, temporal and spatial resolution significantly lag sensors. In this work, we integrate several recent advances in microfluidics and mass spectrometry (MS) to create a sampling and analysis system that has good temporal and spatial resolution but is also readily applied to multicomponent measurements and tuned for detecting different compounds. The system also integrates a microinjection device for delivering chemicals directly to the site of measurement.

Microdialysis and related methods involve implanting a sampling device into tissue, collecting fractions, and then analyzing them by appropriate methods. Use of methods like high-performance liquid chromatography (HPLC), capillary electrophoresis (CE), and MS to analyze the collected fractions allow multiple targets to be measured (see [15,16] for reviews). Historically these methods have not been competitive with sensors with respect to spatial and temporal resolution; however, advances over the past 2 decades have reduced the gap. Temporal resolution is mostly limited by the time required to collect enough sample for analysis. The coupling of microdialysis to miniaturized methods, such as fast capillary LC[17,18], direct infusion MS[19], and CE[20–23], has improved temporal resolution from minutes to a few seconds. Temporal resolution may also become limited by the dispersion of sampled concentration pulses due to flow and diffusion during mass transfer from the sampling device to fraction collector. Collecting samples into segmented flow, where each fraction is compartmentalized into a droplet by an immiscible fluid immediately after sampling, can prevent such dispersion and allow higher temporal resolution[24–26]. This approach has been used for monitoring concentration dynamics *in vitro*[24,27] and *in vivo*[19,25,28], allowing temporal resolution of less than 10 s. Several analytical methods have

been coupled with droplet fraction collection including enzyme assay[25,29], electrochemical detection[30–32], microchip CE[26,28], and MS[24,33–35]. Some of these methods, such as CE and MS, preserve the potential for multicomponent analysis and ready adaption to different analytes.

Spatial resolution of sampling devices has also improved over the original style of microdialysis probes, which are 220 - 400 μm diameter × 1 - 4 mm long. Low-flow push-pull perfusion offers the best spatial resolution[29,36,37]. In this method, two capillaries are fixed side-by-side and sample removed by one capillary while make-up fluid is added through the other capillary at flow rates of 50 - 100 nL/min. Sampling occurs only near the inlet/outlet, thus greatly improving spatial resolution over microdialysis. Sampling areas are approximately 0.02 mm^2 compared to 0.7 - 5 mm^2 for microdialysis. Use of microfabrication allows even smaller probes to be made[38–41]. Microfabricated silicon probes that are 85 μm wide × 70 μm thick containing a 20 μm-square orifices have been reported yielding sampling areas at least 1000-fold smaller than a microdialysis probe[39]. The smaller size is important not only for spatial resolution but also reducing invasiveness of the probes.

Little work however has been done on converging the improved temporal and spatial resolution advances for *in vivo* monitoring. That is, good temporal resolution has been achieved with large probes and better spatial resolution has only been achieved with low temporal resolution. In one exception, a hand assembled low-flow push-pull probe was coupled to droplets which were analyzed by an enzyme assay for glutamate[29]. The system achieved 7 s temporal resolution but was limited to a single analyte. Recent work has shown utility of a microfabricated polymer-based probe (240 μm wide × 86 μm thick) for segmented flow sample pulling prior to a laser ablation inductively coupled plasma MS analysis of metals[42]. This system allowed collection of 18 nL droplets and a temporal resolution of 50 s.

In this work we couple a microfabricated silicon push-pull probe to droplet collection. The microfabricated probe also integrates an injector to allow chemical manipulation of the sampled area. Collected droplets are analyzed by direct infusion nanoelectrospray ionization (nESI) MS. This combination yields samples from a 20 μm × 60 μm area and attains 6 s temporal resolution. nESI MS allows multicomponent measurements (4 analytes together with their internal standard in this case) and potential tuning for different analytes. The resulting integrated system therefore achieves many of the goals of *in vivo* monitoring.

EXPERIMENTAL SECTION

Chemicals and materials

Unless otherwise specified, all chemicals were purchased from Fisher Scientific (Fairlawn, NJ) or Sigma Aldrich (St. Louise, MO) and were certified ACS grade or better. Solutions were prepared with HPLC-grade water, filtered and degassed prior to use. Syringes (Gastight® 1700 Series, 25 μL or 100 μL) were purchased from Hamilton (Reno, NV). Teflon PFA tubing was purchased from IDEX Health & Science (Oak Harbor, WA). Polyimide-coated fused-silica capillary was purchased from Molex (Phoenix, AZ). Fast curing epoxy resins were purchased from Loctite (Westlake, OH) for a standard type and

ITW Devcon (Danvers, MA) for a gel type. Polydimethylsiloxane (PDMS) was purchased from Curbell Plastics (Momentive® RTV 615, Livonia, MI). Crystalbond™ 555 adhesive was purchased from Structure Probe (West Chester, PA). Artificial cerebrospinal fluid (aCSF) consisted of 145 mM NaCl, 2.68 mM KCl, 1.10 mM $MgSO_4$, 1.22 mM $CaCl_2$, 0.50 mM NaH_2PO_4, and 1.55 mM Na_2HPO_4, adjusted pH to 7.4 with 0.1 M NaOH. High-potassium (K^+)-aCSF consisted of 100 mM KCl and 47.7 mM NaCl; the other components were the same as regular aCSF.

Probe and holder

Probes were microfabricated on a 525 μm thick 4-inch silicon wafer (University Wafer, MA) as described in detail elsewhere[39], with modification in probe design. Briefly, a series of microchannels were masked on a wafer by photolithography before the wafer was etched by deep reactive ion etching (DRIE) and XeF_2 etching. The wafer was sealed with poly Si using low pressure chemical vapor deposition. Lithography and DRIE were again used to etch probe shapes and sampling orifices with desired dimensions. The wafer was mounted to a carrier wafer with Crystalbond™ 555 adhesive and backside etched using DRIE prior to probe release in hot water. After probe release, residual adhesive was removed by baking at 610 °C for 8 h in a laboratory kiln.

The final probe size was 11 mm long, 84 μm wide × 70 μm thick. Probes included 3 channels of 20 μm i.d. One channel was used for pull flow. Another channel was used for push flow. The third channel was merged with the push channel at 500 μm from the probe orifice. This additional channel was used for microinjection of a stimulant. Schematics of the probe and its operation are shown in Figure 1 and 2A. For probe handling and sample transfer, a probe was connected to a 5 cm length of 50 μm i.d./150 μm o.d. fused-silica capillaries (“fluidic capillary”) via the use of a probe holder (see Supporting Information, Section I).

Droplet-generator

PDMS microchips were designed to couple the probe outlet to flow segmentation and reagent addition. The PDMS chips were fabricated using a combination of a standard soft lithography technique and a pour over method[43] (see section II of Supporting Information & Figure S-2). A final device contained a 4-way junction (cross) with 125 μm wide × 100 μm tall channels for simultaneous flow segmentation and reagent addition, or a 3-way junction (tee) for flow segmentation only. The devices were designed to create proper sealing and accommodate ease of connection with standard 150 μm o.d. tubing or 360 μm o.d. tubing.

In vitro characterization

Device operation.—The microfabricated probe was operated similar to capillary-based push-pull probes with segmented flow sampling[29]. An outline of the probe integrated with the PDMS chip is illustrated in Figure 2. Push flow was generated from a syringe pump (Chemyx, Stafford, TX) connected to the probe via a 40 cm length of 40 μm i.d. capillary. Pull flow for sampling at 100 nL/min and reagent addition at 55 nL/min (measured by observing droplet size and frequency, and fluorescent intensity) was generated by 200 mm Hg vacuum applied at one arm of the cross that was connected to a length of Teflon tubing

to store collected samples. Other arms were connected to: 1) the probe outlet, 2) a vial of a fluorinated oil (50:1 v/v perfluorodecalin:1H,1H,2H,2H-perfluoro-1-octanol (PFD:PFO), viscosity of 5.1 cps) for flow segmentation, and 3) a mixture of internal standards in water for addition to the sample droplets collected from the probe. The mixture of internal standards included 100 μM ^{13}C-glutamine (Gln), 1 μM ^{13}C-glutamate (Glu), 100 nM ^{13}C-γ-aminobutyric acid (GABA), 20 nM d4-acetylcholine (ACh), and 10 μM fluorescein. For some experiments, the probe outlet was connected to a tee to by-pass addition of internal standards.

Droplet analysis.—Analysis of droplets was carried out using fluorescent microscopy for fluorescein detection and nESI-MS for neurochemical detection. The droplets were pumped from the Teflon storage tubing into a detector using a syringe pump. Fluorescence of droplets were imaged by using an inverted fluorescence microscope (Olympus IX71) with a Xe-arc lamp, appropriate filters, and a CCD camera (Hamamatsu ImageEM X2). When reagent addition was performed, a ratio of added reagents to samples was determined based on the fluorescein intensity in aqueous droplets. For the ESI-MS assay, the outlet end of the Teflon tubing was connected to a nESI tip using a commercial union (PicoClear™, New Objective, Woburn, MA). nESI emitters were made from 50 μm i.d. x 360 μm o.d. fused silica capillary, which was pulled to 15 μm i.d. and platinum coated (FS360-50-15-CE, New Objective, Woburn, MA). Sample droplets were pumped at 50 nL/min through the nESI tip. A potential of +1.25 kV was applied to the Pt coating to induce nESI. Samples were analyzed using a Micromass Quattro Ultima® triple-quadrupole mass spectrometer (Waters, Milford, MA), operated in multiple reaction monitoring (MRM) mode using conditions listed in Table S-1. Data were analyzed by Masslynx 4.1 (Waters, Milfrod, MA). Cutter[44] was used for data processing, peak detection, and determination of peak intensities. Ratio of the peak intensity of each analyte to internal standard intensity was calculated and used for calibration.

In vivo sampling

Surgical procedures were similar to those described previously[40]. Male Sprague-Dawley rats weighting between 250 - 350 g were anesthetized using 2 - 4% isoflurane, and placed in a stereotaxic frame (Kopf Instrument, Tujunga, CA). Animals were maintained under isoflurane over the entire experiment. Probes were stereotaxically inserted to the striatum at coordinates +1.5 mm anterior, ± 3.0 mm lateral to bregma, and a depth of 4.5 mm ventral from dura. Probes were lowered slowly over 1 min. During probe insertion, probe channels were back-flushed at 200 nL/min to prevent clogging before immediately reducing the flow rate to be 100 nL/min at the sampled region. After ~5 min of flow stabilization, an outlet of the pull channel was connected to the PDMS cross before generation of pull flow. For equilibration of baseline, push-pull flow was continued for at least 30 min before sample collection. K^+ stimulation was performed by switching a push flow from aCSF to high K^+-aCSF through the third channel of the probe. High K^+ aCSF was perfused at 100 nL/min for 1 min before switching the flow back to regular aCSF.

For statistical analysis, data were transformed to percentage of baseline. Statistical software R[45] and RStudio in conjunction with the lme4 package[46] were used to perform a linear

mixed-effects analysis of the relationship between baseline percentages of each analyte and phases of stimulations. As fixed effects, phases of stimulations (pre- or post- stimulation) were entered into the model. Animals/subjects were included as random effects. A significance level of 0.05 was used for all analyses. Results were statistically significant when P-value is < 0.05.

RESULTS AND DISCUSSION

Probe and microinjector

Micromachining of silicon was utilized to fabricate push-pull probes as before[39]; however, in this work we sought to increase the yield of probes and to incorporate a microinjector, which is frequently useful in neurochemical experiments. Previously we obtained ~60% yield of useful probes with the majority of failures due to clogging. Clogs were most frequently due to the use of adhesive (Crystalbond™ 555) during the backside etching step that may enter and clog probe channels. To address this problem, we added a step of baking the probes to decompose the adhesive after an initial hot water treatment. Visual inspection showed no visible residue and no effects on performance were found from the heating step. With this step, fabrication yield was improved to 90% (10% of the probes were broken during probe release and manual transfer) of 30 probes tested. Overall, the current fabrication process was reliable, yielding smooth channels with high replication fidelity (see Figure 1B). Processing a single 4-inch wafer yielded about 120 probes.

Microinjection is frequently used to locally add drugs that modulate neural function. Although a separate micropipette can be used, the use of microfabrication allows incorporation of an injector into the device (Figure 1). The two main channels were used for push and pull flow. The additional injector channel was merged with the push channel, creating a tee-junction at 500 μm above the orifice. Switching the flow at the tee junction allowed microinjection of a stimulant. At a flow rate of 100 nL/min, the 10% to 90% rise time of a step concentration change at the probe exit was theoretically estimated to be 72 ms[29]. The time to begin exiting the probe (i.e., the time required to flush the channel volume) was estimated to be 94 ms based on flow rates and channel volumes.

Microfabrication allowed limiting the space between the push and pull orifices to be merely 20 μm (Figure 1B, iii). The active sampling area of the probe, which defines the spatial resolution, was 20 μm × 60 μm. This sampling area is about 10-fold smaller than that of push-pull probe made from capillaries[29]; although somewhat larger than push-pull probes made by pulling glass capillaries to ~30 μm outer diameters[47]. Compared to a conventional microdialysis probe with 2 mm long × 220 μm diameter membrane, spatial resolution of the microfabricated push-pull probe is approximately 1000-fold higher.

Droplet generation and multicomponent measurement by MS

For analytical measurements it is desirable to add reagents or internal standards to collected samples. The microfluidic cross shown in Figure 2 was used to add reagent as sample droplets were formed. Using our conditions, droplets with approximately 1:1.5 aqueous: PFD/PFO volume ratio were generated (see Figure 2B, inset). Sample droplets were about

4.5 nL (formed every ~3 s) and reagent was added at 1:0.55 sample: reagent volume ratio resulting in 7 nL droplets. As shown in Figure 3A, reliable sampling and reagent addition could be attained with an average of 3% RSD in peak height for serial sampling and reagent additions. Regulation of pull flow rates was achieved based on flow resistance of the tubing connected to each arm of the cross. In other words, desired flow rates of sample, PFD/PFO, and reagent could be achieved by selecting appropriate capillary geometries and applied vacuum pressure, and estimated by using the Hagen-Poiseuille equation.

Direct infusion nESI-MS was utilized for analysis of collected droplets. Pilot experiments revealed that low infusion flow rates were necessary to enable detection of the amino acids in aCSF. As shown in Figure 4, decreasing the flow rate of infusion allowed significantly better discrimination against background. This improvement can be attributed to the nanospray effect, i.e. low infusion rates reduce ionization suppression and matrix effects. This is important as the high salt content of aCSF and the complex sample matrix can suppress ionization of other compounds. Therefore, for all assays we used an infusion rate of 50 nL/min.

Using an infusion flow rate of 50 nL/min, droplets were reliably transferred to the nESI tip without coalescence and allowed collection of 7 - 8 data points per droplet during multiple reaction monitoring. Using the microfluidic cross (Figure 2), a stable isotope labeled internal standard of each analyte was added via the reagent addition channel during sample collection. The internal standard allowed for normalizing the effect of matrix and instrument drift on signals.

In this work, we measured 3 neurotransmitters (Glu, GABA and Ach) and Gln, a metabolite of Glu. Temporal resolution and sensitivity of the method were characterized *in vitro* by sampling from a stirred vial of a mixture of the 4 analytes in aCSF. An example of droplet analysis for monitoring Gln is illustrated in Figure 3B. The rise time during concentration change was ~6 s (2 droplets) at a sampling rate of 100 nL/min. This rise time was in agreement with the result using the tee for flow segmentation only (see section I of Supporting Information and Figure S-1). Hence, temporal resolution was not limited by reagent addition, sample storage before analysis (1-3 h), or the MS assay. Calibration curves were obtained with good linearity (R^2 values were >0.95) and the dynamic range covered expected *in vivo* concentrations of each analyte (Figure 3C). The assay was reasonably reproducible with RSDs of the peak intensity ratios in the range of 6 - 11%. Using a signal to noise (peak to peak) ratio of 2, the limits of detection (LODs) were 90 nM for Gln, 60 nM for Glu, 20 nM for GABA, and 2 nM for ACh.

In vivo monitoring of neurotransmitter dynamics

The complete system (microfabricated probe with microinjection, droplet-based microchip with addition of internal standards, and direct infusion MS assay) was used for *in vivo* neurochemical monitoring. Basal concentrations of the analytes were estimated to be 6.4 ± 2.3 μM for Gln, 0.20 ± 0.05 μM for Glu, 62 ± 10 nM for GABA, and 2.3 ± 0.7 nM for ACh (mean ± SEM, n = 4 animals; at least 50 samples for each animal). These concentrations were not corrected for recovery; however, *in vitro* recoveries of the probe were measured to be 83 ± 3%, 47 ± 10%, and 18 ± 7% (n = 5) by sampling fluorescein at a

perfusion rate of 100 nL/min, in a stirred vial, a non-stirred vial, and a 0.6% agarose gel[48], respectively (Figure S-3). The ACh concentrations were near the LOD and therefore this neurotransmitter was not as reliably detected as the others.

In general the sampled concentrations measured in this experiment were lower than those previously reported for the same brain region (see Table S-2 for summary)[19,29,36,39,40,49–60]. Gln is typically found in several hundred micromolar concentrations but we found it to be below 10 μM. The reports for basal concentration of Glu have been variable with a ranges of 1 – 5 μM for sampling studies and 2 - 18 μM for microelectrode studies[51]; however, in this study we observed 0.20 μM. GABA has been reported in the range of 300 – 700 nM while we observed 60 nM. ACh was generally about 30 nM but we observed < 4 nM.

The lower concentrations could be due to a variety of factors. Most significantly, our concentrations are not corrected for recovery as it is not yet known how recovery for low-flow push-pull perfusion is altered *in vivo*. If recovery is similar to sampling from agar gel, where we observed about 18% recovery, then our concentrations would be similar to previous reports. Also, it is possible that pull flow rates during sampling were lower than the nominal 100 nL/min which in turn would lower observed recovery. Although flow *in vivo* was initially set to be 100 nL/min, it is possible that during the experiment clogs developed that slowed the flow. (Lower flow rates of sample would result in droplets that were more diluted by the internal standard solution, which is added at a fixed rate, and appear as a lower concentration of analyte in the droplet. Also, if there is a mismatch in push and pull flow rates, then we may preferentially sample from the push volume and obtain a lower concentration.) Similarly, the excess volume injected during probe lowering (both channels back-flushed at 200 nL/min) might create a volume that dilutes neurotransmitters if it did not dissipate. Other variables that can affect recovered concentrations include anesthesia, probe size, and probe geometry[61].

To demonstrate capability of the system for detection of rapid chemical changes, microinjection of 100 mM K^+-aCSF was performed to stimulate neurochemical release. As shown in Figure 5, microinjections of high K^+ solution evoked transient increases that lasted < 30 s, yet could be captured by this method, for all analytes. For the first injection, the changes at peak maximum from the baselines were 500 ± 120% for Gln, 810 ± 390% for Glu, 1800 ± 1300% for GABA, and 620 ± 280% for ACh (mean ± SEM, n = 4). For a subsequent injection, the average increases were 430 ± 120% for Gln, 330 ± 130% for Glu, 790 ± 500% for GABA, and 300 ± 110 % for ACh. The percent increase in Glu was similar to previous work (see Table S-3 for comparison[20,22,28,29,51,52,55,62]). In addition, substantial effect of K^+ stimulation on GABA levels was also in agreement with the previous studies[28,55,57]. Increases in ACh were also similar to other previous reports[63–65]. However, we observed increases in Gln while other work reported decreases in Gln levels after K^+ stimulation[66–70]. The reasons for this discrepancy are unclear. The other approaches perfused a high-K^+ solution for a much longer time. The prolonged exposure of brain tissues to the solution could alter the dynamics observed[63,71]. Furthermore, the other work used larger probe sizes and collected and analyzed samples at fractions of several minutes. These spatial and temporal differences may ultimately yield different results. Variability observed in the stimulated responses is reasonable; but could be due to a variety of factors including:

1) if rapid changes occurred the temporal resolution may distort them, i.e. we may have insufficient sampling rate; 2) spatial heterogeneity in the brain may result in different responses from the small probe size; 3) complex fluid dynamics may arise from having the injector close to the sampling probe that might cause some variability; and 4) variability in the start of the syringe pump may affect the amount and dynamics of K^+ infusion.

The rise time for K^+ response was 15 ± 3 s. This rise time is slower than the temporal resolution of the monitoring system. The slower rise time was likely due to the use of a syringe pump for microinjections, which typically required at least 5 – 10 s before reaching the desired perfusion rate. Importantly though, these *in vivo* experiments illustrate the capability of the microfabricated probe and analysis system for achieving both high spatiotemporal resolution and multiplexed neurochemical monitoring.

Although the probes cannot sample from single synapses, the spatial resolution should be sufficient for monitoring chemical activity in small brain regions or detecting heterogeneity in larger brain nuclei. The temporal resolution achieved is not sufficient to detect single exocytotic events or release from single action potentials. However, these dynamics will be useful in tracking changes that occur during behaviors and response to rapid stimuli.

The nESI system was sufficiently robust for relatively long term monitoring. Figure 6 illustrates an example of analysis of 400 droplets collected over about 20 min. Such long term measures were routinely achieved.

Operation of the system revealed some areas for improvement in sampling. During *in vivo* experiments, we occasionally observed disturbance of segmented-sampling flow that led to flow blockage or eventual clogging. The origin of the cause of flow disruption is still not clear. The cause of this disruption might be due to tissue debris at the probe inlet[72]. In addition, it is possible that variations in intracranial pressure (caused by several factors, such as surgery procedures and brain exposure to local room pressure[41]), flow rate of CSF[73,74], and viscosity of sampled fluid[75,76] can affect to disturbance of microfluidic flow. Although these variations were not previously reported to be an issue in other low-flow push-pull studies[29,36,62], their negative effects on device operation might become significant in miniaturized sampling with segmented flow (i.e., when active sampling area and fraction volumes are extremely small). Further work is required to understand these effects. Development and use of integrated, automated pressure controller and flow meter will help to accordingly adjust microfluidic flows and overcome the above issue. The use of low flow rates to achieve nano-ESI enabled overcoming ionization suppression sufficient to allow detection of the compounds tested here. Further work will be required to determine if direct infusion will allow detection of other neurotransmitters and metabolites.

CONCLUSION

The combination of microfabricated push-pull sampling probes, flow-segmentation, and direct nano-ESI-MS of droplets yields a system that can achieve 5-10 s temporal resolution for monitoring molecules with a spatial resolution and low invasiveness that is comparable to most sensors while retaining the multiplexing and ability to tune selectivity that is

afforded by MS. Thus this approach achieves several of the important goals for *in vivo* monitoring. It is likely possible to achieve a sub-second temporal resolution with further refinements. Further work is needed to better understand *in vivo* recovery with the probes as well as mitigate causes of flow disturbance. Further work is also required to learn how applicable this approach will be to different chemical targets. The method is limited by the ability to overcome ionization suppression and the sensitivity of the mass spectrometer used. Newer instruments and on-line sample preparation of the droplets should expand the number of analytes detectable by this approach. The use of microfabrication for creating probes is a significant benefit. For example, in this case a microinjector was directly incorporated into the device. In principle it may be possible to integrate other features, such as electrodes for electrophysiological recording. In addition to *in vivo* neurochemical monitoring, the technology developed here maybe adaptable to other microenvironments that require chemical monitoring and drug delivery at high spatiotemporal resolution.

Supplementary Material

Refer to Web version on PubMed Central for supplementary material.

ACKNOWLEDGEMENT

This work was supported by NIH R37 EB003320. We also thank W.H. Lee for initial help with probe design and fabrication processes, staff at the Lurie Nanofabrication Facility (LNF) for technical support, T.R. Slaney for advice about *in vivo* push-pull perfusion sampling, and consultants at the Consulting for Statistics, Computing, and Analytics Research (CSCAR) for assistance with statistical analysis.

REFERENCES

(1). Day JJ; Roitman MF; Wightman RM; Carelli RM Associative Learning Mediates Dynamic Shifts in Dopamine Signaling in the Nucleus Accumbens. Nat. Neurosci 2007, 10 (8), 1020–1028. [PubMed: 17603481]

(2). Wise RA Brain Reward Circuitry: Insights from Unsensed Incentives. Neuron 2002, 36 (2), 229–240. [PubMed: 12383779]

(3). Blouin AM; Fried I; Wilson CL; Staba RJ; Behnke EJ; Lam HA; Maidment NT; Karlsson KÆ; Lapierre JL; Siegel JM Human Hypocretin and Melanin-Concentrating Hormone Levels Are Linked to Emotion and Social Interaction. Nat. Commun 2013, 4, 1547. [PubMed: 23462990]

(4). de la Fuente-Fernández R; Ruth TJ; Sossi V; Schulzer M; Calne DB; Stoessl AJ Expectation and Dopamine Release: Mechanism of the Placebo Effect in Parkinson's Disease. Science 2001, 293 (5532), 1164–1166. [PubMed: 11498597]

(5). Volkow ND; Morales M The Brain on Drugs: From Reward to Addiction. Cell 2015, 162 (4), 712–725. [PubMed: 26276628]

(6). Watson CJ; Venton BJ; Kennedy RT *In Vivo* Measurements of Neurotransmitters by Microdialysis Sampling. Anal. Chem 2006, 78 (5), 1391–1399. [PubMed: 16570388]

(7). Westerink BHC; Cremers TIFH Handbook of Microdialysis: Methods, Applications and Perspectives, 1st ed.; Academic Press, 2007; Vol. 16.

(8). Kennedy RT Emerging Trends in *in Vivo* Neurochemical Monitoring by Microdialysis. Curr. Opin. Chem. Biol 2013, 17 (5), 860–867. [PubMed: 23856056]

(9). Robinson DL; Hermans A; Seipel AT; Wightman RM Monitoring Rapid Chemical Communication in the Brain. Chem. Rev 2008, 108 (7), 2554–2584. [PubMed: 18576692]

(10). Bucher ES; Wightman RM Electrochemical Analysis of Neurotransmitters. Annu. Rev. Anal. Chem 2015, 8 (1), 239–261.

(11). Liang R; Broussard GJ; Tian L Imaging Chemical Neurotransmission with Genetically Encoded Fluorescent Sensors. ACS Chem. Neurosci 2015, 6 (1), 84–93. [PubMed: 25565280]

(12). Lin MZ; Schnitzer MJ Genetically Encoded Indicators of Neuronal Activity. Nat. Neurosci 2016, 19 (9), 1142–1153. [PubMed: 27571193]

(13). Ametamey SM; Honer M; Schubiger PA Molecular Imaging with PET. Chem. Rev 2008, 108 (5), 1501–1516. [PubMed: 18426240]

(14). Finnema SJ; Scheinin M; Shahid M; Lehto J; Borroni E; Bang-Andersen B; Sallinen J; Wong E; Farde L; Halldin C; Grimwood S Application of Cross-Species PET Imaging to Assess Neurotransmitter Release in Brain. Psychopharmacology (Berl.) 2015, 232, 4129–4157. [PubMed: 25921033]

(15). Perry M; Li Q; Kennedy RT Review of Recent Advances in Analytical Techniques for the Determination of Neurotransmitters. Anal. Chim. Acta 2009, 653 (1), 1–22. [PubMed: 19800472]

(16). Saylor RA; Lunte SM A Review of Microdialysis Coupled to Microchip Electrophoresis for Monitoring Biological Events. J. Chromatogr. A 2015, 1382, 48–64. [PubMed: 25637011]

(17). Liu Y; Zhang J; Xu X; Zhao MK; Andrews AM; Weber SG Capillary Ultrahigh Performance Liquid Chromatography with Elevated Temperature for Sub-One Minute Separations of Basal Serotonin in Submicroliter Brain Microdialysate Samples. Anal. Chem 2010, 82 (23), 9611–9616. [PubMed: 21062014]

(18). Gu H; Varner EL; Groskreutz SR; Michael AC; Weber SG *In Vivo* Monitoring of Dopamine by Microdialysis with 1 Min Temporal Resolution Using Online Capillary Liquid Chromatography with Electrochemical Detection. Anal. Chem 2015, 87 (12), 6088–6094. [PubMed: 25970591]

(19). Song P; Hershey ND; Mabrouk OS; Slaney TR; Kennedy RT Mass Spectrometry "Sensor" for in Vivo Acetylcholine Monitoring. Anal. Chem 2012, 84 (11), 4659–4664. [PubMed: 22616788]

(20). O'Shea TJ; Weber PL; Bammel BP; Lunte CE; Lunte SM; Smyth MR Monitoring Excitatory Amino Acid Release *in Vivo* by Microdialysis with Capillary Electrophoresis- Electrochemistry. J. Chromatogr. A 1992, 608 (1), 189–195.

(21). Parrot S; Sauvinet V; Riban V; Depaulis A; Renaud B; Denoroy L High Temporal Resolution for *in Vivo* Monitoring of Neurotransmitters in Awake Epileptic Rats Using Brain Microdialysis and Capillary Electrophoresis with Laser-Induced Fluorescence Detection. J. Neurosci. Methods 2004, 140 (1–2), 29–38. [PubMed: 15589331]

(22). Tucci S; Rada P; Sepúlveda MJ; Hernandez L Glutamate Measured by 6-s Resolution Brain Microdialysis: Capillary Electrophoretic and Laser-Induced Fluorescence Detection Application. J. Chromatogr. B. Biomed. Sci. App 1997, 694 (2), 343–349.

(23). Lada MW; Vickroy TW; Kennedy RT High Temporal Resolution Monitoring of Glutamate and Aspartate *in Vivo* Using Microdialysis On-Line with Capillary Electrophoresis with Laser-Induced Fluorescence Detection. Anal. Chem 1997, 69 (22), 4560–4565. [PubMed: 9375517]

(24). Chen D; Du W; Liu Y; Liu W; Kuznetsov A; Mendez FE; Philipson LH; Ismagilov RF The Chemistrode: A Droplet-Based Microfluidic Device for Stimulation and Recording with High Temporal, Spatial, and Chemical Resolution. Proc. Natl. Acad. Sci 2008, 105 (44), 16843–16848. [PubMed: 18974218]

(25). Wang M; Roman GT; Schultz K; Jennings C; Kennedy RT Improved Temporal Resolution for *in Vivo* Microdialysis by Using Segmented Flow. Anal. Chem 2008, 80 (14), 5607–5615. [PubMed: 18547059]

(26). Wang M; Roman GT; Perry ML; Kennedy RT Microfluidic Chip for High Efficiency Electrophoretic Analysis of Segmented Flow from a Microdialysis Probe and *in Vivo* Chemical Monitoring. Anal. Chem 2009, 81 (21), 9072–9078. [PubMed: 19803495]

(27). Easley CJ; Rocheleau JV; Head WS; Piston DW Quantitative Measurement of Zinc Secretion from Pancreatic Islets with High Temporal Resolution Using Droplet-Based Microfluidics. Anal. Chem 2009, 81 (21), 9086–9095. [PubMed: 19874061]

(28). Wang M; Slaney T; Mabrouk O; Kennedy RT Collection of Nanoliter Microdialysate Fractions in Plugs for Off-Line *in Vivo* Chemical Monitoring with up to 2s Temporal Resolution. J. Neurosci. Methods 2010, 190 (1), 39–48. [PubMed: 20447417]

(29). Slaney TR; Nie J; Hershey ND; Thwar PK; Linderman J; Burns MA; Kennedy RT Push–Pull Perfusion Sampling with Segmented Flow for High Temporal and Spatial Resolution *in Vivo* Chemical Monitoring. Anal. Chem 2011, 83 (13), 5207–5213. [PubMed: 21604670]

(30). Liu S; Gu Y; Roux RBL; M. Matthews S; Bratton D; Yunus K; C. Fisher A; S. Huck WT The Electrochemical Detection of Droplets in Microfluidic Devices. Lab. Chip 2008, 8 (11), 1937–1942. [PubMed: 18941696]

(31). Han Z; Li W; Huang Y; Zheng B Measuring Rapid Enzymatic Kinetics by Electrochemical Method in Droplet-Based Microfluidic Devices with Pneumatic Valves. Anal. Chem 2009, 81 (14), 5840–5845. [PubMed: 19518139]

(32). Rogers M; Leong C; Niu X; de Mello A; Parker KH; Boutelle MG Optimisation of a Microfluidic Analysis Chamber for the Placement of Microelectrodes. Phys. Chem. Chem. Phys 2011, 13 (12), 5298. [PubMed: 21344092]

(33). Fidalgo LM; Whyte G; Ruotolo BT; Benesch JLP; Stengel F; Abell C; Robinson CV; Huck WTS Coupling Microdroplet Microreactors with Mass Spectrometry: Reading the Contents of Single Droplets Online. Angew. Chem. Int. Ed 2009, 48 (20), 3665–3668.

(34). Li Q; Pei J; Song P; Kennedy RT Fraction Collection from Capillary Liquid Chromatography and Off-Line Electrospray Ionization Mass Spectrometry Using Oil Segmented Flow. Anal. Chem 2010, 82 (12), 5260–5267. [PubMed: 20491430]

(35). Zhu Y; Fang Q Integrated Droplet Analysis System with Electrospray Ionization-Mass Spectrometry Using a Hydrophilic Tongue-Based Droplet Extraction Interface. Anal. Chem 2010, 82 (19), 8361–8366. [PubMed: 20806885]

(36). Kottegoda S; Shaik I; Shippy SA Demonstration of Low Flow Push–Pull Perfusion. J. Neurosci. Methods 2002, 121 (1), 93–101. [PubMed: 12393165]

(37). Pritchett JS; Pulido JS; Shippy SA Measurement of Region-Specific Nitrate Levels of the Posterior Chamber of the Rat Eye Using Low-Flow Push−Pull Perfusion. Anal. Chem 2008, 80 (14), 5342–5349. [PubMed: 18549240]

(38). Zahn JD; Trebotich D; Liepmann D Microdialysis Microneedles for Continuous Medical Monitoring. Biomed. Microdevices 2005, 7 (1), 59–69. [PubMed: 15834522]

(39). Lee WH; Slaney TR; Hower RW; Kennedy RT Microfabricated Sampling Probes for *in Vivo* Monitoring of Neurotransmitters. Anal. Chem 2013, 85 (8), 3828–3831. [PubMed: 23547793]

(40). Lee WH; Ngernsutivorakul T; Mabrouk OS; Wong J-MT; Dugan CE; Pappas SS; Yoon HJ; Kennedy RT Microfabrication and *in Vivo* Performance of a Microdialysis Probe with Embedded Membrane. Anal. Chem 2016, 88 (2), 1230–1237. [PubMed: 26727611]

(41). Petit-Pierre G; Bertsch A; Renaud P Neural Probe Combining Microelectrodes and a Droplet-Based Microdialysis Collection System for High Temporal Resolution Sampling. Lab Chip 2016, 16 (5), 917–924. [PubMed: 26864169]

(42). Petit-Pierre G; Colin P; Laurer E; Déglon J; Bertsch A; Thomas A; Schneider BL; Renaud P In Vivo Neurochemical Measurements in Cerebral Tissues Using a Droplet-Based Monitoring System. Nat. Commun 2017, 8 (1), 1239. [PubMed: 29093476]

(43). Guetschow ED; Steyer DJ; Kennedy RT Subsecond Electrophoretic Separations from Droplet Samples for Screening of Enzyme Modulators. Anal. Chem 2014, 86 (20), 10373–10379. [PubMed: 25233947]

(44). Shackman JG; Watson CJ; Kennedy RT High-Throughput Automated Post-Processing of Separation Data. J. Chromatogr. A 2004, 1040 (2), 273–282. [PubMed: 15230534]

(45). R Core Team. R: A Language and Environment for Statistical Computing; R Foundation for Statistical Computing: Vienna, Austria, 2017.

(46). Bates D; Mächler M; Bolker B; Walker S Fitting Linear Mixed-Effects Models Using Lme4. ArXiv14065823 Stat 2014.

(47). Cabay MR; McRay A; Featherstone DE; Shippy SA Development of μ-Low-Flow-Push–Pull Perfusion Probes for Ex Vivo Sampling from Mouse Hippocampal Tissue Slices. ACS Chem. Neurosci 2018, 9 (2), 252–259. [PubMed: 29077383]

(48). Chen Z-J; Gillies GT; Broaddus WC; Prabhu SS; Fillmore H; Mitchell RM; Corwin FD; Fatouros PP A Realistic Brain Tissue Phantom for Intraparenchymal Infusion Studies. J. Neurosurg 2004, 101 (2), 314–322. [PubMed: 15309925]

(49). Kennedy RT; Thompson JE; Vickroy TW *In Vivo* Monitoring of Amino Acids by Direct Sampling of Brain Extracellular Fluid at Ultralow Flow Rates and Capillary Electrophoresis. J. Neurosci. Methods 2002, 114, 39–49. [PubMed: 11850038]

(50). Yamamoto BK; Davy S Dopaminergic Modulation of Glutamate Release in Striatum as Measured by Microdialysis. J. Neurochem 1992, 58 (5), 1736–1742. [PubMed: 1348523]

(51). Oldenziel WH; Dijkstra G; Cremers TIFH; Westerink BHC *In Vivo* Monitoring of Extracellular Glutamate in the Brain with a Microsensor. Brain Res. 2006, 1118 (1), 34–42. [PubMed: 16956598]

(52). Day BK; Pomerleau F; Burmeister JJ; Huettl P; Gerhardt GA Microelectrode Array Studies of Basal and Potassium-Evoked Release of l-Glutamate in the Anesthetized Rat Brain. J. Neurochem 2006, 96 (6), 1626–1635. [PubMed: 16441510]

(53). Massieu L; Morales-Villagrán A; Tapia R Accumulation of Extracellular Glutamate by Inhibition of Its Uptake Is Not Sufficient for Inducing Neuronal Damage: An *In Vivo* Microdialysis Study. J. Neurochem 1995, 64 (5), 2262–2272. [PubMed: 7722511]

(54). Kanamori K; Ross BD Quantitative Determination of Extracellular Glutamine Concentration in Rat Brain, and Its Elevation in Vivo by System A Transport Inhibitor, α-(Methylamino)Isobutyrate: Elevation of Brain GLNECF by MeAIB in Vivo. J. Neurochem 2004, 90 (1), 203–210. [PubMed: 15198679]

(55). Wang M; Hershey ND; Mabrouk OS; Kennedy RT Collection, Storage, and Electrophoretic Analysis of Nanoliter Microdialysis Samples Collected from Awake Animals *in Vivo*. Anal. Bioanal. Chem 2011, 400 (7), 2013–2023. [PubMed: 21465093]

(56). Slaney TR; Mabrouk OS; Porter-Stransky KA; Aragona BJ; Kennedy RT Chemical Gradients within Brain Extracellular Space Measured Using Low Flow Push–Pull Perfusion Sampling in Vivo. ACS Chem. Neurosci 2013, 4 (2), 321–329. [PubMed: 23421683]

(57). Ciriacks Klinker C; Bowser MT 4-Fluoro-7-Nitro-2,1,3-Benzoxadiazole as a Fluorogenic Labeling Reagent for the *in Vivo* Analysis of Amino Acid Neurotransmitters Using Online Microdialysis−Capillary Electrophoresis. Anal. Chem 2007, 79 (22), 8747–8754. [PubMed: 17929877]

(58). Huang T; Yang L; Gitzen J; Kissinger PT; Vreeke M; Heller A Detection of Basal Acetylcholine in Rat Brain Microdialysate. J. Chromatogr. B Biomed. Appl 1995, 670 (2), 323–327. [PubMed: 8548023]

(59). Ichikawa J; Dai J; O'Laughlin IA; Fowler WL; Meltzer HY Atypical, but Not Typical, Antipsychotic Drugs Increase Cortical Acetylcholine Release without an Effect in the Nucleus Accumbens or Striatum. Neuropsychopharmacol. Off. Publ. Am. Coll. Neuropsychopharmacol 2002, 26 (3), 325–339.

(60). Herrera-Marschitz M; You Z-B; Goiny M; Meana JJ; Silveira R; Godukhin OV; Chen Y; Espinoza S; Pettersson E; Loidl CF; Lubec G; Andersson K; Nylander I; Terenius L; Ungerstedt U On the Origin of Extracellular Glutamate Levels Monitored in the Basal Ganglia of the Rat by *in Vivo* Microdialysis. J. Neurochem 1996, 66 (4), 1726–1735. [PubMed: 8627331]

(61). Patterson SL; Sluka KA; Arnold MA A Novel Transverse Push–Pull Microprobe: *In Vitro* Characterization and *in Vivo* Demonstration of the Enzymatic Production of Adenosine in the Spinal Cord Dorsal Horn. J. Neurochem 2001, 76 (1), 234–246. [PubMed: 11145997]

(62). Cellar NA; Burns ST; Meiners J-C; Chen H; Kennedy RT Microfluidic Chip for Low-Flow Push-Pull Perfusion Sampling *in Vivo* with On-Line Analysis of Amino Acids. Anal. Chem 2005, 77 (21), 7067–7073. [PubMed: 16255611]

(63). Marien MR; Richard JW Drug Effects on the Release of Endogenous Acetylcholine *In Vivo*: Measurement by Intracerebral Dialysis and Gas Chromatography–Mass Spectrometry. J. Neurochem 1990, 54 (6), 2016–2023. [PubMed: 2338554]

(64). Arenas E; Alberch J; Arroyos RS; Marsal J Effect of Opioids on Acetylcholine Release Evoked by K+ or Glutamic Acid from Rat Neostriatal Slices. Brain Res. 1990, 523 (1), 51–56. [PubMed: 1976420]

(65). Moore H; Stuckman S; Sarter M; Bruno JP Potassium, but Not Atropine-Stimulated Cortical Acetylcholine Efflux, Is Reduced in Aged Rats. Neurobiol. Aging 1996, 17 (4), 565–571. [PubMed: 8832631]

(66). Girault JA; Barbeito L; Spampinato U; Gozlan H; Glowinski J; Besson M-J In *Vivo* Release of Endogenous Amino Acids from the Rat Striatum: Further Evidence for a Role of Glutamate and Aspartate in Corticostriatal Neurotransmission. J. Neurochem 1986, 47 (1), 98–106. [PubMed: 2872275]

(67). Molchanova S; Kööbi P; Oja SS; Saransaari P Interstitial Concentrations of Amino Acids in the Rat Striatum During Global Forebrain Ischemia and Potassium-Evoked Spreading Depression. Neurochem. Res 2004, 29 (8), 1519–1527. [PubMed: 15260129]

(68). Segovia G; Porras A; Mora F Effects of 4-Aminopyridine on Extracellular Concentrations of Glutamate in Striatum of the Freely Moving Rat. Neurochem. Res 1997, 22 (12), 1491–1497. [PubMed: 9357015]

(69). Morales-Villagrán A; Tapia R Preferential Stimulation of Glutamate Release by 4-Aminopyridine in Rat Striatum *in Vivo*. Neurochem. Int 1996, 28 (1), 35–40. [PubMed: 8746762]

(70). Westerink BHC; Damsma G; Rollema H; De Vries JB; Horn AS Scope and Limitations of *in Vivo* Brain Dialysis: A Comparison of Its Application to Various Neurotransmitter Systems. Life Sci. 1987, 41 (15), 1763–1776. [PubMed: 2889121]

(71). Kawasaki K; Czéh G; Somjen GG Prolonged Exposure to High Potassium Concentration Results in Irreversible Loss of Synaptic Transmission in Hippocampal Tissue Slices. Brain Res. 1988, 457 (2), 322–329. [PubMed: 2851366]

(72). Peterson SL; McDonald A; Gourley PL; Sasaki DY Poly(Dimethylsiloxane) Thin Films as Biocompatible Coatings for Microfluidic Devices: Cell Culture and Flow Studies with Glial Cells. J. Biomed. Mater. Res. A 2005, 72A (1), 10–18.

(73). Reiber H Flow Rate of Cerebrospinal Fluid (CSF)--a Concept Common to Normal Blood-CSF Barrier Function and to Dysfunction in Neurological Diseases. J. Neurol. Sci 1994, 122 (2), 189–203. [PubMed: 8021703]

(74). Reiber H Proteins in Cerebrospinal Fluid and Blood: Barriers, CSF Flow Rate and Source-Related Dynamics. Restor. Neurol. Neurosci 2003, 21 (3,4), 79–96. [PubMed: 14530572]

(75). Brydon HL; Hayward R; Harkness W; Bayston R Physical Properties of Cerebrospinal Fluid of Relevance to Shunt Function. 1: The Effect of Protein upon CSF Viscosity. Br. J. Neurosurg 1995, 9 (5), 639–644. [PubMed: 8561936]

(76). Brydon HL; Keir G; Thompson EJ; Bayston R; Hayward R; Harkness W Protein Adsorption to Hydrocephalus Shunt Catheters: CSF Protein Adsorption. J. Neurol. Neurosurg. Psychiatry 1998, 64 (5), 643–647. [PubMed: 9598681]

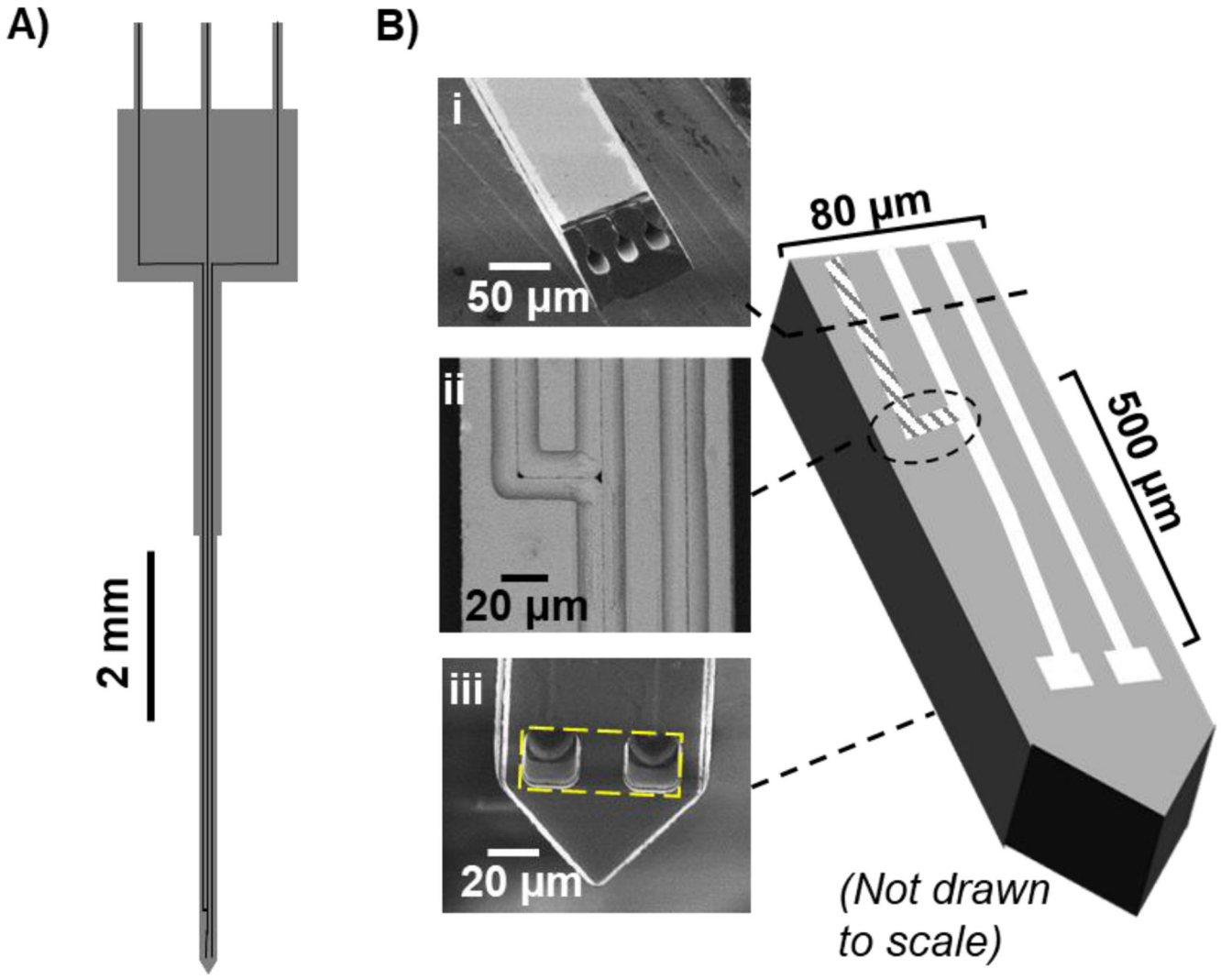

Figure 1.

A) Overview of probe shape and channels. B) SEM images of microfabricated push pull probe with additional channel for microinjection. The images show i) cross section of the probe; ii) top view of an integrated tee (after backside etch to reveal the channels); iii) tip of the probe with an estimated sampling area (yellow dashed).

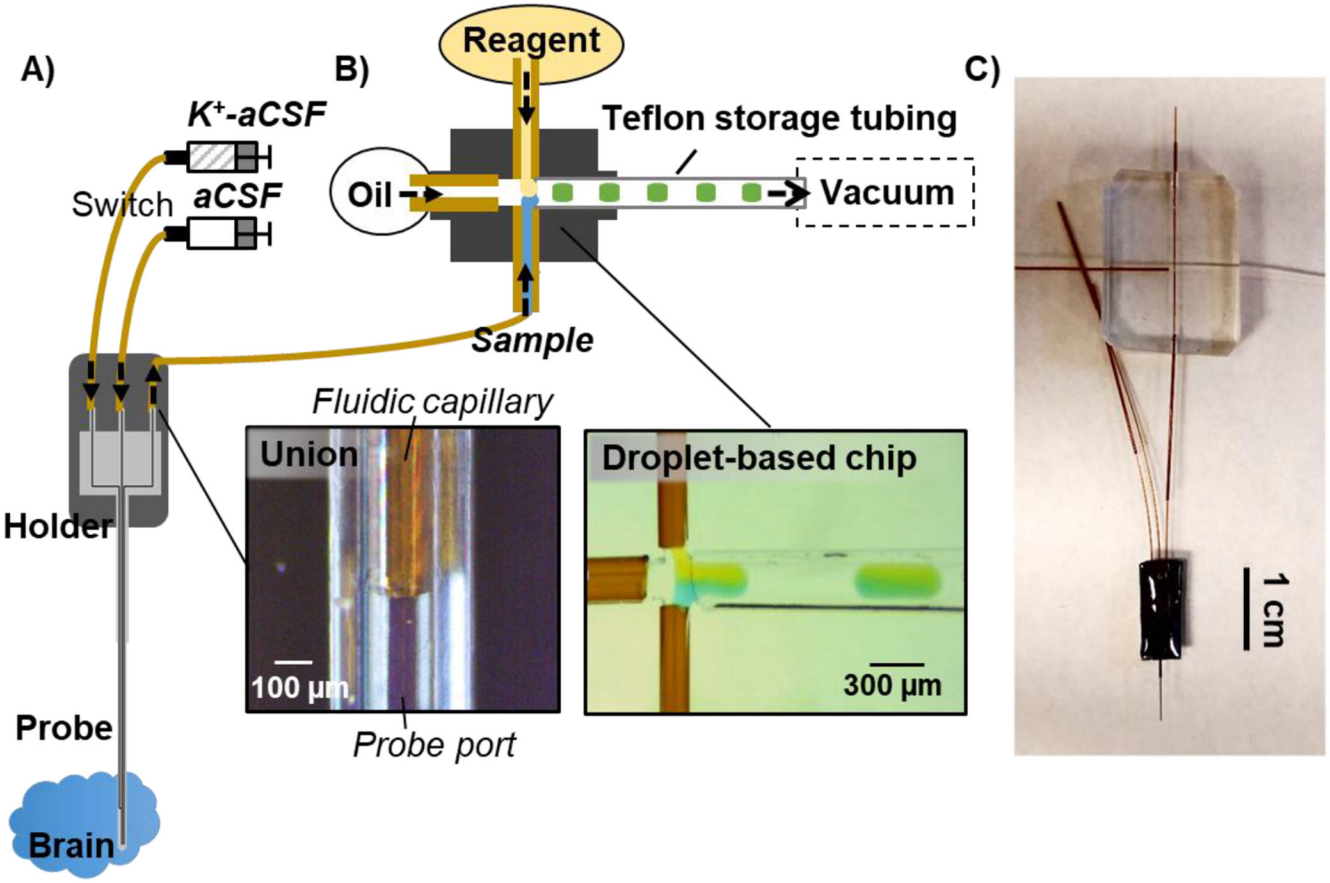

Figure 2.

Overview of experimental setup for monitoring brain chemical dynamics with high spatiotemporal resolution. A) microfabricated push-pull probe with 3 channels. The first and second channels were used for pushing regular aCSF and microinjection of K^+-aCSF. The last channel was used for pulling sample. The inset showed microfluidic interface between the probe and a “fluidic” capillary. This capillary was used for sample transfer prior to connecting with a microfabricated cross for simultaneous flow segmentation and reagent addition (B). Generated droplets were collected in a Teflon storage tubing prior to an offline analysis. The inset showed a microscopic photograph of the flow segmentation with reagent addition. Food dyes were added to sample and reagent for visualization. C) Photograph of the probe connected to the droplet-based device.

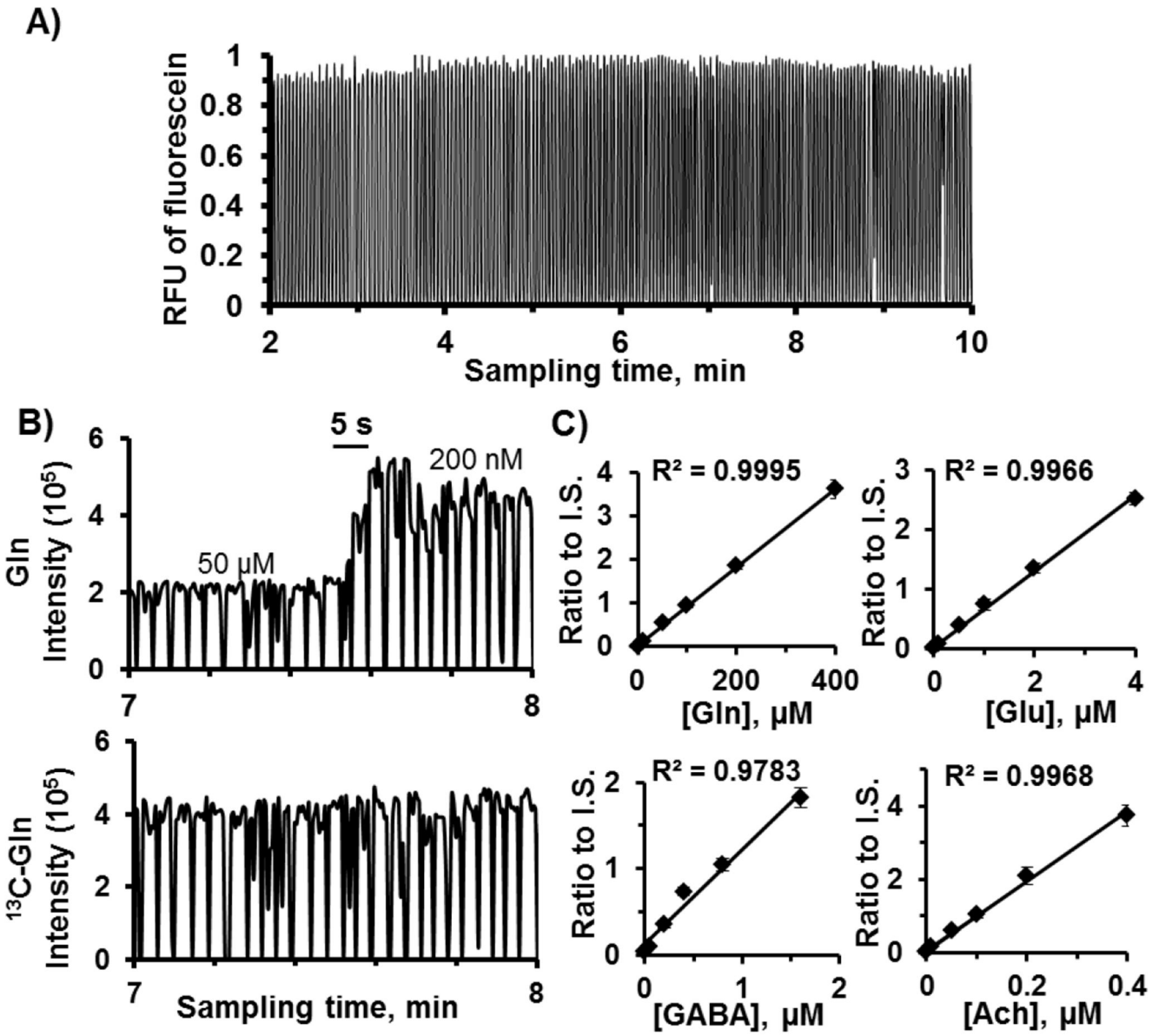

Figure 3.

In vitro characterization of sampling coupled to segmented flow and reagent addition. Samples were a mixture of standards in aCSF and reagents contained fluorescein and a mixture of internal standards. A) Detection of fluroescein in droplets yielded peak heights with RSD of 3% (n = 3 device sets). An example of a step change of ACh during switching concentration is shown in (B) along with related internal standard added at the same period. C) Calibration curves from ratio of signal traces of standards to internal standards. Linear calibration curves were achieved.

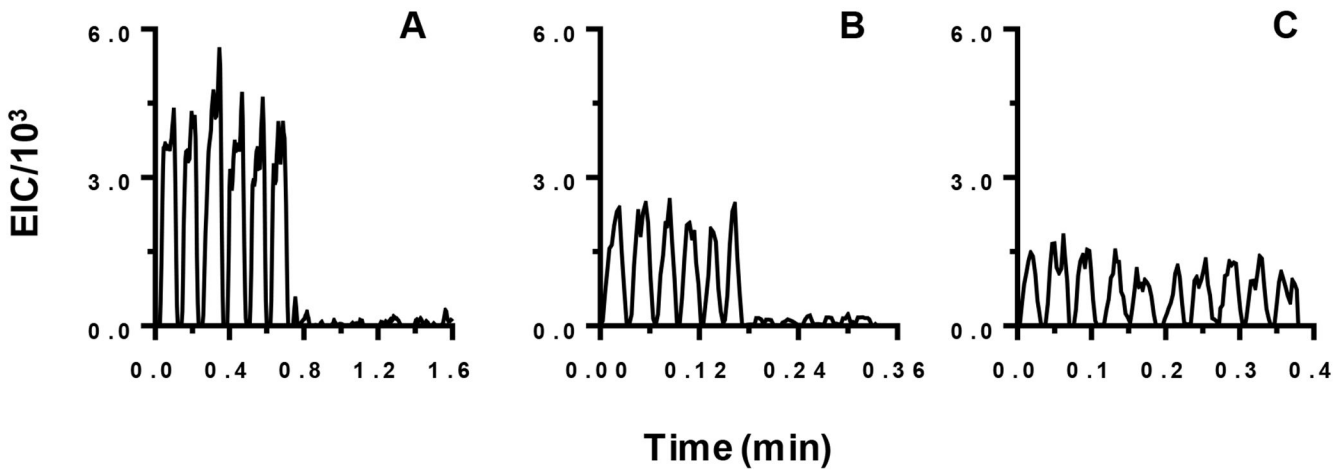

Figure 4.

Comparison of signals obtained for MS/MS of 1 μM GABA dissolved in aCSF at (A) 50 nL/min; (B) 300 nL/min; and (C) 800 nL/min. Each trace shows the signal intensity for the 104 → 87 m/z transition for 10 droplets. The first 5 contained GABA and the last 5 were aCSF only. For (A) and (B) each droplet was 4 nL and spaced by 4 nL carrier fluid. For (C) each droplet was 10 nL spaced by 10 nL carrier fluid.

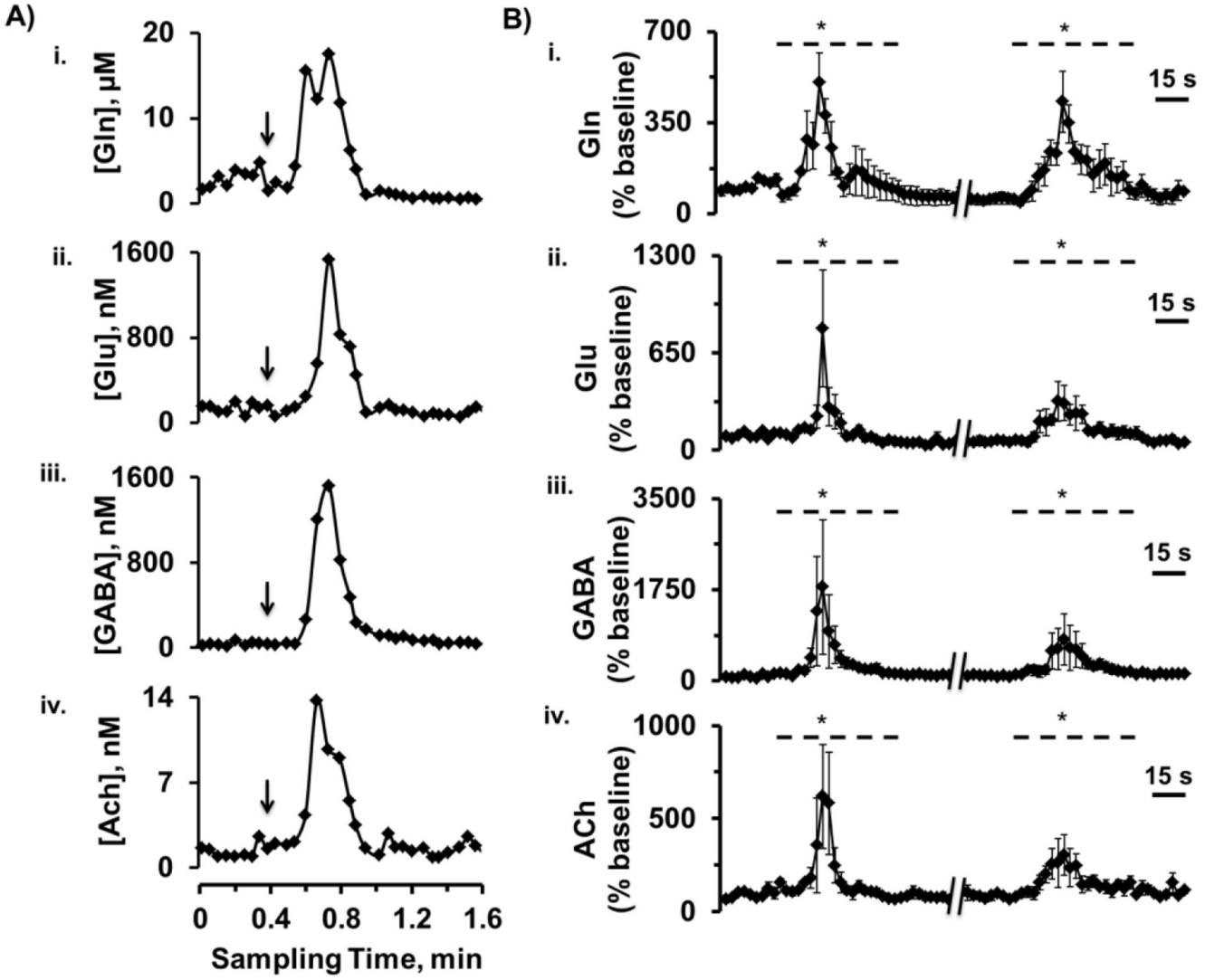

Figure 5.

In vivo monitoring of response to microinjection of 100 mM K^+-aCSF in the rat striatum. (A) shows an example trace for simultaneous responses of Gln (i), Glu (ii), GABA (iii) and ACh (iv). Arrows indicate beginning of microinjection. Rise times could be observed within 3 droplets or ~9 s. (B) shows averaged responses of Gln (i), Glu (ii), GABA (iii) and ACh (iv), (mean ± SEM, n = 4 rats). Data were expressed as percentages of the averaged baseline values during pre-stimulation levels. Dashed lines indicate periods of K^+-stimulation. Linear-mixed effects models indicate significant changes (*, $p < 0.05$) between basal and stimulation phases.

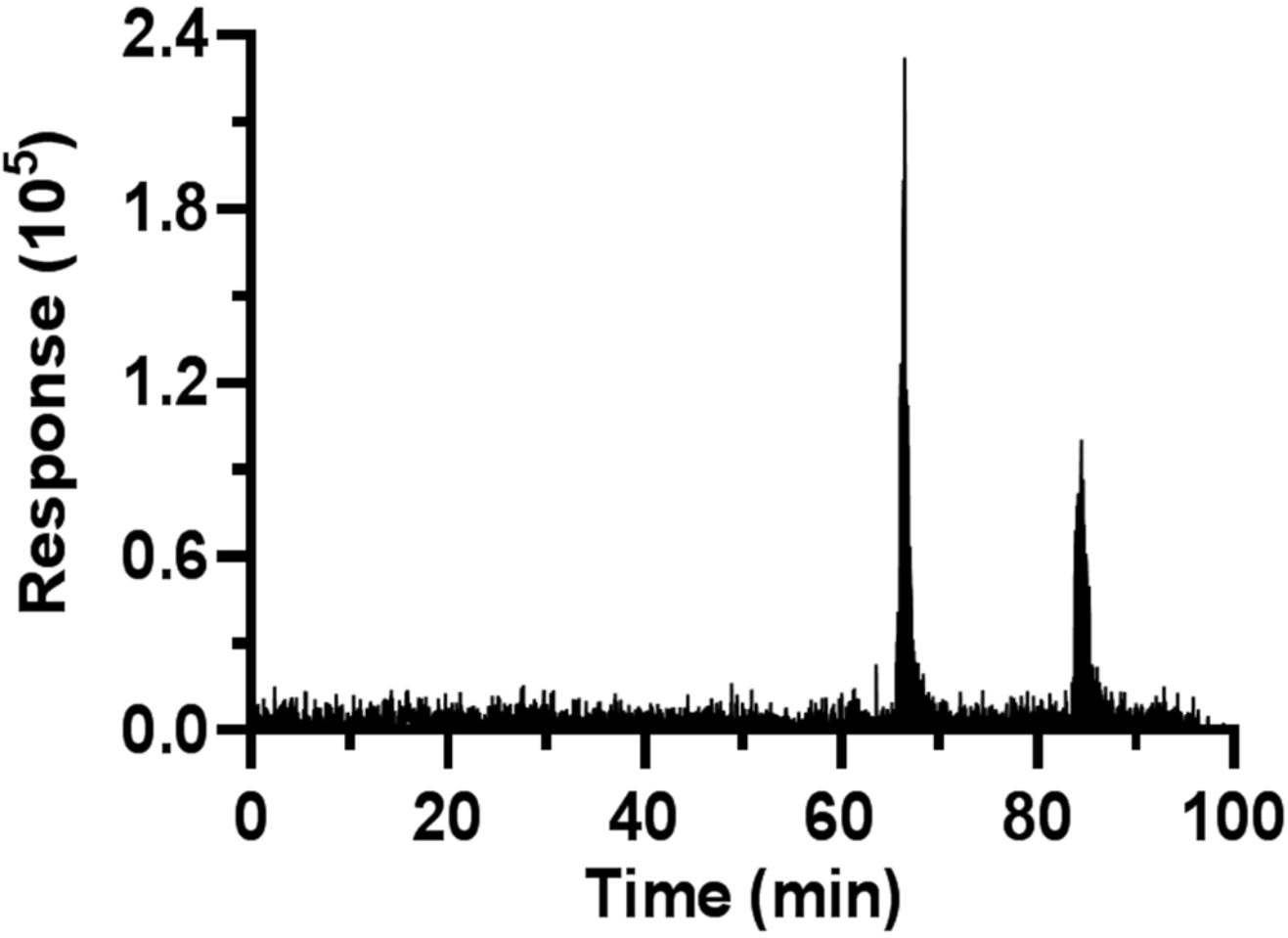

Figure 6.

Raw MS/MS data for GABA from *in vivo* collection. ~4.5 nL brain samples (volume was ~7 nL after addition of internal standard) were infused with segmenting fluid at 50 nL/min for 100 min, corresponding to about 400 samples. The two increases in signal correspond to K^+ infusions. Time axis is time for analysis and is not corrected to sampling time.